Nonreciprocal quantum transport at junctions of structured leads

Eduardo Mascarenhas,[1] François Damanet,[1] Stuart Flannigan,[1] Luca Tagliacozzo,[1,2] Andrew J. Daley,[1] John Goold,[3] and Inés de Vega[4]

[1]*Department of Physics and SUPA, University of Strathclyde, Glasgow G4 0NG, Scotland, United Kingdom*

[2]*Departament de Física Quàntica i Astrofísica and Institut de Ciències del Cosmos (ICCUB), Universitat de Barcelona, Martí i Franquès 1, 08028 Barcelona, Catalonia, Spain*

[3]*School of Physics, Trinity College Dublin, The University of Dublin, College Green Dublin 2, Ireland*

[4]*Physics Department and Arnold Sommerfeld Center for Theoretical Physics, Ludwig-Maximilians-Universitat Munchen, D-80333 Munchen, Germany*

(Received 18 January 2019; revised manuscript received 10 April 2019; published 19 June 2019)

We propose and analyze a mechanism for rectification of spin transport through a small junction between two spin baths or leads. For interacting baths, we show that transport is conditioned on the spacial asymmetry of the quantum junction mediating the transport, and attribute this behavior to a gapped spectral structure of the lead-system-lead configuration. For noninteracting leads, a minimal quantum model that allows for spin rectification requires an interface of only two interacting two-level systems. In our paper, we have performed a thorough study of the current, including its time dependence and steady-state value. We obtain approximate results with a weak-coupling Born master equation in excellent agreement with matrix-product-state calculations that are extrapolated in time by mimicking absorbing boundary conditions. These results should be observable in controlled spin systems realized with cold atoms, trapped ions, or in electrons in quantum dot arrays.

DOI: 10.1103/PhysRevB.99.245134

I. INTRODUCTION

Recent experimental developments in solid-state and atomic physics have opened opportunities to explore properties of quantum transport in and out of equilibrium [1–7]. One important element of quantum transport is the possibility to generate rectification of currents, or nonreciprocal transport, that is, currents whose magnitude depends on the bias direction. Such phenomena may arise from *asymmetry* and *nonlinearity* in the underlying dynamics—on a quantum mechanical level, effective nonlinearity is associated with interactions between particles [8]. In recent years, the study and design of systems that rectify transport has continuously expanded into the quantum regime; for example, in optical systems [9–25] and spin models [26–40]. Most of the recent literature has focused on phenomenological Markovian baths that drive the system of interest, and spin rectification was demonstrated for XXZ systems with asymmetric coupling along the Z axis [32,33,37]. The ZZ couplings correspond to density-density interactions, as the system can be mapped to spin-less interacting fermions. The presence of such interactions is believed to be paramount for the presence of rectification of the spin current.

In this paper. we address the problem of controlling transport between two many-body systems. In this setting, non-Markovian effects [41–48] are naturally expected. We adopt an open system approach beyond the Markov approximation to analyze a nonequilibrium many-body problem. Two interacting leads modeled as XXZ spin chains are coupled by a small interface, the open system, as depicted in Fig. 1(a). For a *noninteracting* interface, we present a mechanism for rectification of spin currents, which arises from the *spectral structure* of the leads [see Fig. 1(d)]. We also show that for structureless leads, a noninteracting system is fully reciprocal in agreement with the previous literature. Conversely, for structureless baths, a minimal model allowing for efficient rectification requires a junction of two *interacting* spins.

Before addressing rectification of the spin current, we establish the accuracy and efficiency of the open system approach and show that the (non-Markovian) Born weak-coupling master equation governing the dynamics of the small junction is in excellent agreement with matrix-product-state (MPS) simulations of the global dynamics. The sudden connection between system and leads generates two light cones, a weak and fast moving cone and a strong and slow moving cone. As a byproduct, we extend MPS simulations by mimicking absorbing boundaries that dissipate the weak light cone. The Born equation is determined by the first-order correlations of the leads, which decay as power laws in XXZ spin chains [49,50]. Since such slow decay is a generic feature of many-body systems [51], the effects reported here could be observed in a variety of difference systems, including trapped atoms [1–3], ions [4,5], and superconducting leads coupled to quantum dots [6,7,52].

II. MODEL AND TRANSPORT

We first discuss the general transport properties. As depicted in Fig. 1(a), we consider left and right leads coupled to an interface with a coupling Hamiltonian given by

$$V = V_L + V_R, \quad V_i = 2\gamma[B_i S_i^\dagger + B_i^\dagger S_i], \tag{1}$$

where $B_{L(R)}$ are left (right) bath operators at the junction coupled with the corresponding system operators $S_{L(R)}$. The

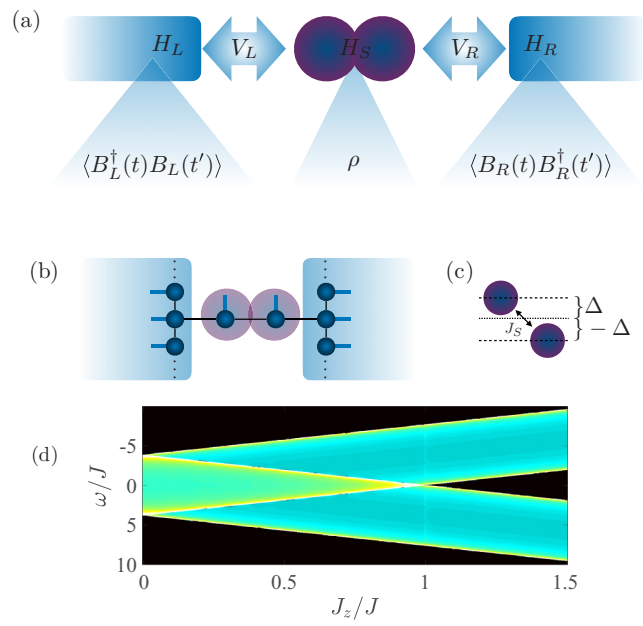

FIG. 1. (a) Representation of bath-system-bath coupling and effective evolution of the central interface that depends on its past history and time correlations of the bath. (b) The system-lead state $|\Psi\rangle$ depicted as a matrix product state reflecting the corresponding Hamiltonian structure of bulk-coupling. (c) The small asymmetric interface between the leads is represented as a two-qubit structure. (d) The system-bath asymptotic nonequilibrium spectral function $A_\Pi(\omega)$ under the Born approximation for different J_z couplings showing the spectral structure of the bath with a gap around $\omega = 0$ for certain regimes in the limit $H_S \ll H_B$ ($J_S, \gamma = 0.01J$).

system-bath coupling strength γ is assumed to be small compared to the system's and baths' frequency scales. The global dynamics are then governed by $\dot{\rho}_{SB} = -i[H_S + H_B + V, \rho_{SB}]$, with H_S the system Hamiltonian and $H_B = H_L + H_R$ the sum of left and right lead Hamiltonians.

In an interaction picture, we define $\widetilde{V}(t) = e^{iH_0 t} V e^{-iH_0 t}$, with $H_0 = H_S + H_B$ dictating the dynamics of the combined system-bath density matrix $\widetilde{\rho}_{SB}$. A system operator O (that commutes with H_S for simplicity) follows a continuity Heisenberg equation from which we define the current operator at the left (L) system-bath junction $\frac{dO}{dt}|_L = j_L^{(O)} = i[V_L, O]$. Its average value may be written in a second-order iterated form,

$$I_L(t) = \mathrm{tr}\{\rho_{SB}(t) j_L^{(O)}\} = -i \int_0^t dt' \langle [\tilde{j}_L^{(O)}(t), \widetilde{V}(t')] \rangle_{t'}, \quad (2)$$

in which we have eliminated the first-order term for convenience (this is exact for the cases we address here). A similar expression follows for the current at the right junction. Note that Eq. (2) is exact and requires solving the system-bath many-body dynamics since $\langle \cdots \rangle_{t'} = \mathrm{tr}\{\cdots \rho_{SB}(t')\}$. We will focus on 1/2-spin transport such that $O = Z = S^\dagger S - S S^\dagger$, leading to the spin-current operator:

$$j_L^{(Z)} = j_L = i[V_L, Z_L] = -i4\gamma [B_L S_L^\dagger - S_L B_L^\dagger]. \quad (3)$$

Equation (2) can be rewritten as $I_L(t) = -i8\gamma^2 \int_0^t dt' \Pi_L(t, t')$, in terms of the nonequilibrium two-particle retarded-Green's function [53]:

$$\begin{aligned}\Pi_L(t,t') = &-i\Theta(t-t')\langle \widetilde{B}_L(t)\widetilde{B}_L^\dagger(t')\widetilde{S}_L^\dagger(t)\widetilde{S}_L(t')\\ &- \widetilde{B}_L^\dagger(t)\widetilde{B}_L(t')\widetilde{S}_L(t)\widetilde{S}_L^\dagger(t')\\ &+ \widetilde{B}_L(t)\widetilde{B}_R^\dagger(t')\widetilde{S}_L^\dagger(t)\widetilde{S}_R(t')\\ &- \widetilde{B}_L^\dagger(t)\widetilde{B}_R(t')\widetilde{S}_L(t)\widetilde{S}_R^\dagger(t') + \mathrm{H.c.}\rangle_{t'}. \quad (4)\end{aligned}$$

The total average current flowing through the system is defined as $I(t) = [I_L(t) - I_R(t)]/2 = -i8\gamma^2 \int_0^t dt' \Pi(t, t')$, with the total Green's function $\Pi = [\Pi_L - \Pi_R]/2$. The asymptotic current can be expressed as

$$\begin{aligned}I(\infty) &= -i\frac{8\gamma^2}{\sqrt{2\pi}} \int_{-\infty}^{\infty} dt' \int_{-\infty}^{\infty} d\omega e^{i\omega t'} \Pi(\omega)\\ &= 8\gamma^2 A_\Pi(0), \quad (5)\end{aligned}$$

where we have defined the joint nonequilibrium spectral function as $A_\Pi(\omega) = -\mathrm{Im}\{\Pi(\omega)\}$ with $\Pi(\omega)$ being the Fourier transform of $\Pi(\infty, t')$ [in practice the asymptotic behavior is captured by $\Pi(t' + \infty, \infty)$]. Therefore, $A_\Pi(0)$ plays a similar role to a generalized zero-frequency conductivity.

III. WEAK-COUPLING APPROXIMATIONS

So far, the expressions derived for the current are exact. However, to proceed further, it is convenient to consider approximations to the global system-bath state. One possibility is to use the Kubo approximation [53–56], which assumes that the weak perturbation only causes a small change in the global system-bath state $\widetilde{\rho}_{SB}(t) \approx \widetilde{\rho}_{SB}(0) + \gamma f(t)$. Although this is a good approach for the state of the baths, it can be a poor approximation for the state of the small interface. The Born ansatz takes this into account and allows the system to evolve by considering that the global state is $\widetilde{\rho}_{SB}(t) \approx \widetilde{\rho}_S(t) \otimes [\widetilde{\rho}_B(0) + \gamma f(t)]$. With Kubo's linear response theory [53–56], the quantum average in Eq. (4) is substituted by $\langle \cdots \rangle_{00} = \mathrm{tr}\{\cdots \rho_{SB}(0)\}$. Similarly, with the Born ansatz, the average becomes $\langle \cdots \rangle_{t'0} = \mathrm{tr}\{\cdots \widetilde{\rho}(t') \otimes \rho_B(0)\}$. These approximations assume that terms of order higher then γ^2 can be neglected. Also note that the Kubo approximation to the Green's function Eq. (4) factors the first term (for example) into $\langle \widetilde{B}_L(t)\widetilde{B}_L^\dagger(t')\rangle_0 \langle \widetilde{S}_L^\dagger(t)\widetilde{S}_L(t')\rangle_0$, while the Born approximation leads to $\langle \widetilde{B}_L(t)\widetilde{B}_L^\dagger(t')\rangle_0 \langle \widetilde{S}_L^\dagger(t)\widetilde{S}_L(t')\rangle_{t'}$. Both approximations neglect correlations between system and bath, but also the correlations that emerge between different baths mediated by the system. Thus, the last two terms of Eq. (4) are dropped [57].

With the Born ansatz, tracing over the bath degrees of freedom we may compute the evolution for the system state [58,59]. Dropping the subindex for the system state we have the Born master equation,

$$\begin{aligned}\dot{\widetilde{\rho}} = -4\gamma^2 \int_0^t dt' \sum_i \big[&\langle \widetilde{B}_i^\dagger(t)\widetilde{B}_i(t')\rangle \widetilde{S}_i(t)\widetilde{S}_i^\dagger(t')\widetilde{\rho}(t')\\ &+ \langle \widetilde{B}_i(t)\widetilde{B}_i^\dagger(t')\rangle \big(\widetilde{S}_i^\dagger(t)\widetilde{S}_i(t')\widetilde{\rho}(t') - \widetilde{S}_i(t')\widetilde{\rho}(t')\widetilde{S}_i^\dagger(t)\big)\\ &- \langle \widetilde{B}_i^\dagger(t)\widetilde{B}_i(t')\rangle \widetilde{S}_i^\dagger(t')\widetilde{\rho}(t')\widetilde{S}_i(t) + \mathrm{H.c.}\big], \quad (6)\end{aligned}$$

with the bath correlations dictating the dynamics of the system with memory effects as illustrated in Fig. 1(a). Computing the

long time evolution of the system state via Eq. (6) can still be time-consuming due to the integral-differential nature of the equation of motion and the show power-law decay of bath correlations. An exact Redfield master equation can be derived directly targeting the Born steady state (see Appendix B). A phenomenological approach that leads to a Lindblad form [60–63] can be used far away from the spectral gap.

IV. EXAMPLE OF AN XXZ BATH

We consider the leads (left and right) to both be described by XXZ spin-1/2 chains, with a Hamiltonian of the form

$$H_{\rm XXZ}^{L(R)} = \sum_{r=-\infty}^{\infty} 2J\left[\sigma_r^{L(R)\dagger}\sigma_{r+1}^{L(R)} + \sigma_{r+1}^{L(R)\dagger}\sigma_r^{L(R)}\right] + J_z^{(\rm bath)} Z_r^{L(R)} Z_{r+1}^{L(R)}, \tag{7}$$

with $Z_r = \sigma_r^\dagger\sigma_r - \sigma_r\sigma_r^\dagger$, with $\sigma_r = |0\rangle_r\langle 1|_r$ and J and J_z the coupling strengths.

The interface system is composed by two coupled asymmetric spins as represented in Fig. 1(c), with the Hamiltonian

$$H_S = 2J_S(\sigma_L\sigma_R^\dagger + \sigma_L^\dagger\sigma_R) + \Delta(Z_L - Z_R) + J_z^{(\rm system)} Z_L Z_R, \tag{8}$$

where Δ is the relative detuning between the spins. As shown in Fig. 1(b), the left (right) system spin couples to a single spin of the left (right) lead. This is described with a Hamiltonian of the form Eq. (1) with $S_{L(R)} = \sigma_{L(R)}$ and $B_{L(R)} = \sigma_0^{L(R)}$.

We analyze a *nonequilibrium* protocol in which the left (−) and right (+) leads are prepared at zero temperature with a large bias $\pm\sum_r \mu Z_r$ added to their respective Hamiltonians while the system is initially prepared in an arbitrary state. Thus a global product state between the system and the leads is prepared with the leads oppositely maximally polarized. Then the bias is turned off and the global system is allowed to evolve generating spin currents. The infinite bias limit also allows us to obtain analytical results. The infinite bias also probes the system in a highly nonlinear regime prone to present rectification. Both the currents and rectification would vanish as the bias goes to zero. The system behaves effectively linearly at low bias as it maps to a Luttinger liquid. In this case, the basic ingredient for rectification is absent. Here, we focus on the maximally biased case and we did not include any analysis for low bias that deviates from the central case study.

In the infinite bias limit, analytic results can be drawn under the first-order Holstein-Primakoff transformation for the baths [64] $Z_r^{L(R)} = 2[1 - a_r^{L(R)\dagger}a_r^{L(R)}]$ and $\sigma_r^{L(R)} = -\sqrt{2}a_r^{L(R)\dagger}$. Under this approximation, the Hamiltonian of the baths take the quadratic form

$$H_{\rm XXZ}^{L(R)} \approx -2\sum_r J\left[a_r^{L(R)\dagger}a_{r+1}^{L(R)} + \text{H.c.}\right] + 2J_z a_r^{L(R)\dagger}a_r^{L(R)}. \tag{9}$$

The corresponding correlation function obeys $\langle B_L^\dagger(t)B_L(0)\rangle = e^{i4J_z^{\rm bath}t}\mathcal{J}_0(4Jt)$, with $\mathcal{J}_0$ being the zeroth-order Bessel function. This result was confirmed by exact MPS simulations (see Appendix C).

Consequently, the decay rate that governs the relaxation dynamics of the interface can be written as

$$\Gamma(\omega) = \gamma^2\int_0^\infty d\tau e^{i\omega\tau}\langle B_L^\dagger(\tau)B_L(0)\rangle = i\gamma^2[(4J_z + \omega + i0^+)^2 - (4J)^2]^{-1/2}, \tag{10}$$

for each system transition of energy ω. The decay rate may diverge, for example, at $\omega = 0$ and $J_z = J$, which could invalidate the perturbative approximation [65]. The divergence can be avoided by slightly detuning the system away from the singularity. For the particular case addressed here, all transitions with $\omega = E' - E = 0$ ($H_S|E\rangle = E|E\rangle$) are forbidden due to the symmetry $\langle E'|S_i|E\rangle = 0$, thus ensuring the validity of the perturbative approach even at singular points.

V. ABSORBING BOUNDARIES

Using MPS simulations represented in Fig. 1(b), similar to Refs. [66–76], we find that the resulting dynamics are in great agreement with master equation for weak coupling. However, such regime produces very slow system relaxation that demands very large leads to prevent boundary reflections, rendering the simulations quickly unfeasible. To prevent this, we incorporate dissipation mechanisms in the baths mimicking absorbing boundary conditions (see Appendix A). This allows for a considerable extension of the time scales reachable by MPS simulations. The current light cones in the leads with and without the absorbing boundaries are compared in Fig. 2.

VI. CURRENTS, SPECTRAL FUNCTIONS AND RECTIFICATION

When the system Hamiltonian is a small perturbation (the limit $H_S \to 0$) the transport is largely governed by the physics of the bath. Generically, we expect ballistic transport for $J_z < J$ with nonzero asymptotic currents, while diffusive or insulating behavior is expected for $J_z > J$ with vanishing asymptotic currents. If $H_S = 0$, the zero-frequency spectral function follows the bath spectral function and we have $A_\Pi \approx A_{\rm XXZ}$ with

$$A_{\rm XXZ}(\omega = 0) = \text{Re}\{[2\pi(J^2 - J_z^2)]^{-1/2}\}/2, \tag{11}$$

for $\mu \gg J$ which is shown in Fig. 2. Thus $I(\infty)$ increases with $J_z^{(\rm bath)}$ up to the Heisenberg point and then suddenly vanishes for $J_z^{(\rm bath)} > J$ with the gap opening of $A_{\rm XXZ}(\omega)$ around $\omega = 0$. In Fig. 1(d), we show the full *system-bath* asymptotic nonequilibrium spectral function $A_\Pi(\omega)$ under the Born approximation with the gap opening for $J_z^{(\rm bath)} > J$ in agreement with the above analysis for the bath spectral function.

In Fig. 2, we compare the different approximations to the current. The MPS simulation shows an initial current burst that is also captured by the Kubo and Born approaches. The relaxation of the system state after this burst is captured by the Born approach while ignored by Kubo. Although reliable, the Born evolution is time-consuming. The steady-state properties are then captured by the long time limit of the Born equation (dark dashed line), which amounts to a single algebraic equation to be solved (Appendix B). The long time

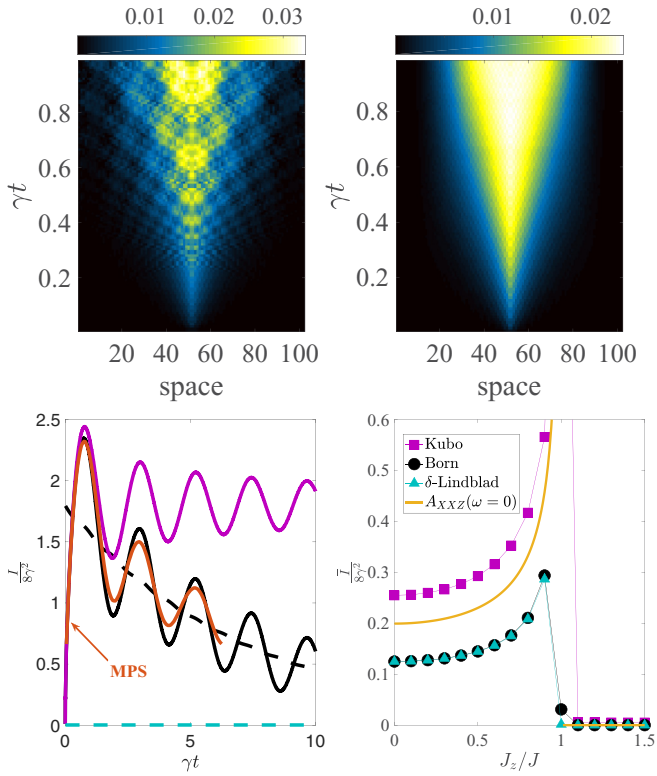

FIG. 2. Currents at each bond in one of the leads without (top left) and with (top right) absorbing boundaries for $J_z = J$, $J_z^{\text{system}} = 0$ and $J_S = \Delta = \gamma = 0.01J$. Reflection from the boundaries are suppressed in the right panel. Bottom left: The MPS, Kubo, and Born spin currents as a function of time at the Heisenberg point $J = J_z^{\text{bath}}$. The dark-dashed line corresponds to Eq. (B1) and the light-dashed line to Eq. (B3). Bottom right: The corresponding asymptotic currents. Parameters are $J_z^{\text{system}} = 0$ and $J_S = \Delta = \gamma = 0.01J$.

currents are shown in Fig. 2 in agreement with the qualitative analysis of A_{XXZ}. The discrepancy between Kubo and the Born steady state results is significant whenever the currents are finite and is more drastic at the Heisenberg point, in which the spectral function is far from constant.

The asymmetry parameter Δ of the system interface can induce nonreciprocal currents. To analyze this, we define the rectification associated to the total spin transported,

$$R_\Delta(T) = \frac{\bar{I}_\Delta(T) - \bar{I}_{-\Delta}(T)}{\bar{I}_\Delta(T) + \bar{I}_{-\Delta}(T)}, \tag{12}$$

such that $\bar{I}_\Delta = \frac{1}{T}\int_0^T I_\Delta(t')dt'$ corresponds to the average current at a given asymmetry Δ. There is usually a trade-off between the rectification factor and the current, in the sense that increasing the asymmetry might lead to higher R; however, it usually also decreases the current since the sites become more and more out of tune [9–11]. Thus, as a last definition we have the diode factor $D_\Delta = \bar{I}_{\text{sign}(R_\Delta)\Delta} R_\Delta$ that captures this trade-off and provides an overall fraction of the current that is rectified.

As seen in Fig. 2, the simple Kubo approach provides an effective upper bound for the current, allowing for a qualitative description of the rectification mechanism. Analyzing the Kubo version of A_Π at zero frequency and at the Heisenberg point, we have a simple expression for the rectification factor,

$$R_\Delta^{\text{Kubo}}(t \approx 1/\gamma) = \Delta\left[J_S^2 + \Delta^2\right]^{-1/2}, \tag{13}$$

for $J_S, \Delta \ll J = J_z \ll \mu$. In Fig. 3, we show that $A_\Pi(0)$ is asymmetric with respect to Δ. In the perturbative limit $J_S \to 0$, a positive Δ leads to a gapless spectral function, while a negative Δ leads to the open gap yielding perfect rectification $R = 1$. A finite J_S leads to a smooth crossover in A_Π while still presenting finite rectification. In Fig. 3, we also show the high rectification factor and the diode factor, accounting for the trade-off between asymmetry and total output current.

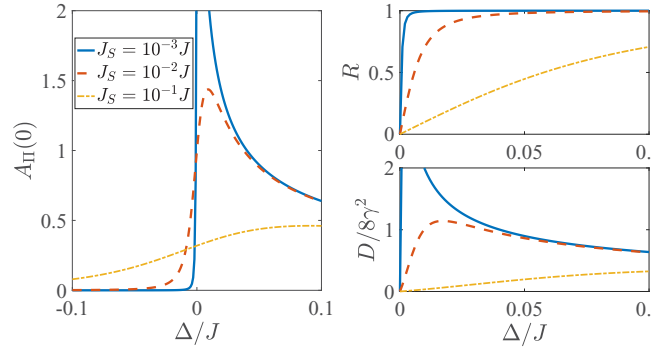

FIG. 3. Analytical Kubo results for the short time response. Left: The joint spectral function. Upper right: The rectification factor and (lower-right) the diode factor. Parameters are $J_z = J$.

The Kubo results are very accurate for short times; however, for long times we have to resort to the Born approach in Fig. 4. For weak system Hamiltonian, a rectification peak manifests just before the Heisenberg point (before the gap opening) as expected by the Kubo analysis (left panel of Fig. 4). Increasing the magnitude of the system Hamiltonian shifts this peak toward lower bath-interactions, indicating that the global spectral gap is shifted by the system Hamiltonian. Higher currents flow from the spin with positive frequency to the spin of negative frequency. In the opposite case of interacting interface and noninteracting leads, the results are markedly different (right panel in Fig. 4). The optimal transport direction is inverted and higher currents flow from

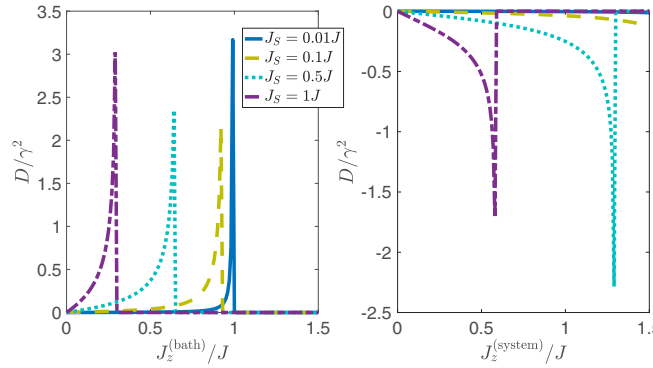

FIG. 4. Asymptotic Born results for the diode factor for (left) a noninteracting system with interacting leads and (right) an interacting-system with noninteracting leads. We set $\Delta = J_S$.

the negative-frequency spin to the positive one. We emphasize that the above results are only captured by the Born approach, which accounts for the dependency of the system dynamics on the spectral properties. In contrast, the local Lindblad equation only considers a single decay rate (i.e., decay channel) for the system and therefore fails for structured baths, particularly when the system frequencies are spread, i.e., when $J_S \approx J$ (see Appendix B).

VII. CONCLUSION

In summary, we have analyzed in detail weak-coupling approximations for transport scenarios which are far from equilibrium, showing how the Born approach goes well beyond linear response and is in good agreement with exact MPS results. Considering a setting with a small system between two XXZ leads, we have shown the presence of nonreciprocal transport. We have presented a mechanism for optimal rectification associated to the asymmetric spectral structure of system+bath induced by the system spacial imbalance. Our results indicate that phenomenological Lindblad approaches may fail since they do not take into account the spectral structure. Lastly, the mapping of the bath to a noninteracting model suggests that rectification may emerge for structured baths even in complete absence of interactions.

The data corresponding to the article is made available by the University of Strathclyde [77].

ACKNOWLEDGMENTS

E.M. thanks Thierry Giamarchi, Ignacio Cirac, Mari-Carmen Banuls, Daniel Valente, and Thiago Werlang for inspiring discussions. Work at the University of Strathclyde was supported by the EPSRC Programme Grant DesOEQ (No. EP/P009565/1), and by the EOARD via AFOSR Grant No. FA9550-18-1-0064. This work was supported by an SFI-Royal Society University Research Fellowship (J.G.). This project received funding from the European Research Council (ERC) under the European Union's Horizon 2020 research and innovation program (Grant Agreement No. 758403). I.D.V. was financially supported by the Nanosystems Initiative Munich (NIM) under Project No. 862050-2 and the DFG Grant No. GZ: VE 993/1-1.

APPENDIX A: ABSORBING-BOUNDARIES MPS SIMULATIONS

Simulating absorbing boundary conditions in classical physics is a relatively simple task typically accomplished by setting derivatives to zero at the boundary. In quantum mechanics, this is still an open problem, in general, with some remarkable strategies for infinite-boundary-MPS simulations [75]. This strategy uses an infinite-MPS algorithm to compute the ground state, such as that presented in Ref. [74]. The authors of Ref. [75] then create a localized perturbation in the center of the i-MPS and evolve the state using a finite-MPS time-evolution algorithm. The only difference in the time evolution is how the sites at the boundary are treated.

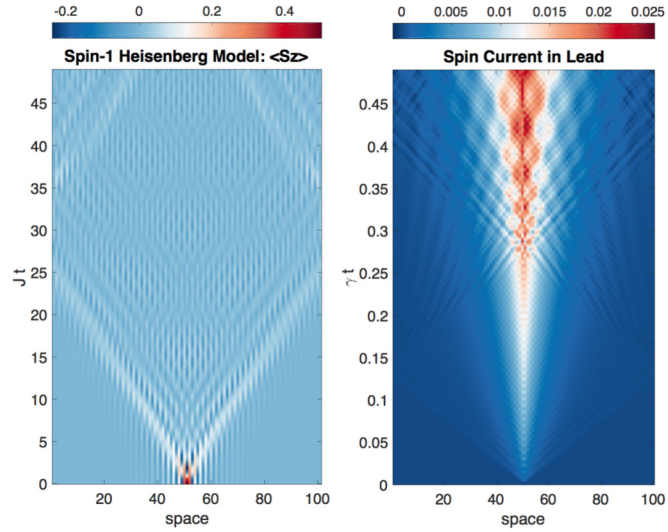

FIG. 5. Infinite boundary MPS (IBMPS) results. Spin projection along z axis for the antiferromagnetic spin-1 Heisenberg model of 100 spins (left) after applying a spin creation operator at site 51, ($\sigma_{51}^{\dagger}$). Spin current at each bond in one of the leads for our open-system model (right). Reflection from the boundaries are delayed but not suppressed.

These need to be evolved by an effective Hamiltonian that takes into account the half infinite boundaries. In Ref. [75], the scheme is applied to the spin-1 Heisenberg model in the antiferromagnetic phase and they show that the perturbation is absorbed by the boundary, allowing them to evolve a smaller system for longer without worrying about boundary effects. However, this strategy fails for the setting considered here. In Fig. 5 (left), we apply this algorithm to the same system as the authors of Ref. [75], i.e., the spin-1 Heisenberg model. The only difference is that we evolve the system with TDVP instead of TEBD. We show that while the perturbation is initially absorbed by the boundary, after evolving to longer times we do still see a reflected component. This delay in the reflection is not enough to allow us to evolve an open-system model for a significantly longer time.

The situation gets worse when we apply this scheme to our open-system model, i.e., two sites coupled to two large leads where the leads are initially in a product state and the Hamiltonian is the spin-1/2 XXZ model. In Fig. 5 (right), we see that at the boundary of one of the leads, there is almost no delay in the reflection of the current, meaning that there is no advantage over simply using a finite-MPS algorithm. The analysis indicates that the success of the strategy of Ref. [75] is highly dependent on the system and specific application. And while it indeed has great potential in some circumstances, as shown by their calculation of the lowest excitation branch of the spin-1 Heisenberg model [75], it is not applicable in the context presented here. This analysis justifies the need to develop a different approach to absorbing boundary conditions.

We include dissipative processes into the original dynamics

$$d|\Psi\rangle = \left[-iHdt - \sum_r \left(\frac{1}{2}J_r^{\dagger}J_r dt - J_r dQ_r\right)\right]|\Psi\rangle, \quad \text{(A1)}$$

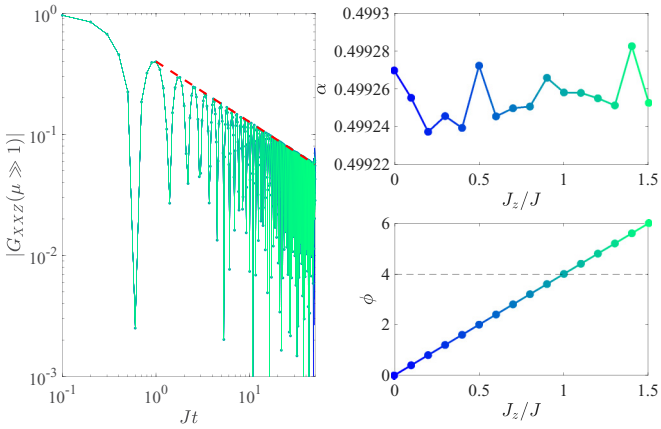

FIG. 6. MPS results for correlations with a chain of 200 spins in agreement with the analytical results. Darker colors correspond to lower J_z while brighter colors correspond to higher J_z. The modulus of the correlation in log-log scale for (upper left) $\mu \gg 1$. The red dashed line is the asymptotic expression in Eq. (C2), respectively. The Bessel function result is indistinguishable from the MPS results. Upper right: The fitted power-law exponent and (lower right) the corresponding phase frequency, assuming $G_{\mathrm{XXZ}} \sim e^{i\phi t} t^{-\alpha}$. Thus we have confirmation that $\alpha = 1/2$ and $\phi = 4J_z$.

with $H = H_S + H_B + V$ and $dQ_r = \langle J_r^\dagger + J_r \rangle dt + dW_r$, with dW_r being Wiener process [78]. These dissipative processes are an auxiliary tool to absorb excitation in the bath and prevent their reflection at the boundary. The J_r operators have to be chosen for the specific problem and there is no general recipe for constructing them. On the left lead, which is prepared in an all up state, we set $J_r = \sqrt{\zeta(r)}\sigma_r^\dagger$ and on the opposite side we set $J_r = \sqrt{\zeta(r)}\sigma_r$ with $\zeta(r) = e^{-\gamma_B r}$ with r being the distance from the boundary and γ_B the effective range of these dissipative processes.

As can be seen in the right panel of Fig. (5), the sudden contact between the system and the lead generates two light cones. One which is weaker and travels as fast as the bath quasiparticles and one which is stronger but much slower. The strategy we have presented here absorbs the first light cone. The second light cone cannot be absorbed faithfully. Therefore, the absorbing boundaries do extend the time span of the MPS simulations (here we observe a factor of at least 4) but do not offer a route to capture the steady state.

APPENDIX B: STEADY STATE MASTER EQUATIONS

Assuming that the bath correlations do decay, no matter how slow, and that consequently the system reaches a steady state, we have the long time limit of the Born master equation,

$$\dot{\rho}(t \to \infty) = 0 = -i[H_S, \rho] - \sum_{s,\omega,\omega',\alpha,\alpha'} \Big[\Gamma^{(s)}_{\alpha,\alpha'}(\omega')\big(K^{(s)\dagger}_{\alpha}(\omega) K^{(s)}_{\alpha'}(\omega')\rho - K^{(s)}_{\alpha'}(\omega')\rho K^{(s)\dagger}_{\alpha}(\omega)\big) + \mathrm{H.c.}\Big], \tag{B1}$$

with $\Gamma^{(s)}_{\alpha,\alpha'}(\omega) = \gamma^2 \int_0^\infty d\tau e^{i\omega\tau} \langle \widetilde{X}^{(s)}_{\alpha}(\tau) \widetilde{X}^{(s)}_{\alpha'}(0)\rangle$, whose real part is an effective relaxation rate and imaginary part a system frequency ω [59]. We have assumed the eigendecomposition $H_S = \sum_E EP(E)$, $P(E) = |E\rangle\langle E|$ with

$$K^{(s)}_{\alpha}(\omega) = \sum_{E'-E=\omega} P(E) K^{(s)}_{\alpha} P(E'), \tag{B2}$$

$K^{(s)}_{\alpha} = i^\alpha [S_s^\dagger + (-1)^\alpha S_s]$, and $X^{(s)}_{\alpha} = (-i)^\alpha [B_s + (-1)^\alpha B_s^\dagger]$ with $\alpha = 0, 1$. The master Eq. (B1) is commonly referred to as the *global* approach since it contains the K operators which can be delocalized in space; however, it is not of Lindblad form since we have not discarded terms that couple different frequencies $\omega \neq \omega'$. Alternatively, *phenomenological* assumptions of the form $\langle \widetilde{B}_i^\dagger(t) \widetilde{B}_i(t')\rangle \approx \Gamma_h^{(i)} \delta(t - t')$ and $\langle \widetilde{B}_i(t) \widetilde{B}_i^\dagger(t')\rangle \approx \Gamma_p^{(i)} \delta(t - t')$ lead to the zero frequency *local* approach,

$$\dot{\rho}_{t\to\infty} \approx -i[H_S, \rho] - \sum_s \big[\Gamma_p^{(s)}(S_s^\dagger S_s \rho - S_s \rho S_s^\dagger) + \mathrm{H.c.}\big] - \sum_s \big[\Gamma_h^{(s)}\big(S_s S_s^\dagger \rho - S_s^\dagger \rho S_s\big) + \mathrm{H.c.}\big], \tag{B3}$$

with $\Gamma_h^{(s)} = 4\gamma^2 \int_0^\infty d\tau \langle \widetilde{B}_s^\dagger(\tau) \widetilde{B}_s(0)\rangle$ and $\Gamma_p^{(s)} = 4\gamma^2 \int_0^\infty d\tau \langle \widetilde{B}_s(\tau) \widetilde{B}_s^\dagger(0)\rangle$. Note that $\Gamma_h^{(s)}$ and $\Gamma_p^{(s)}$ can be expressed in terms of the zero frequency $\Gamma^{(s)}_{\alpha,\alpha'}(\omega = 0)$. Hence, the phenomenological Lindblad approach described in Eq. (B3) is only accurate when the system frequencies are not spread in comparison to the bath spectral function, in such a way that the decay rates corresponding to each system decay channel $\Gamma^{(s)}_{\alpha,\alpha'}(\omega)$ in Eq. (B1) can be well approximated by a single one $\Gamma^{(s)}_{\alpha,\alpha'}(\omega) \approx \Gamma^{(s)}_{\alpha,\alpha'}(\omega = 0)$. Taking into account the multiple decay channels of the system appears to be crucial not only to describe transport properties, as described here, but also to describe thermalization [60–63].

APPENDIX C: TIME CORRELATIONS

Let us start by determining the bath correlations beginning with cases that can be quickly solved analytically, that is, the noninteracting XX model with $J_z = 0$ [51]. To describe the bulk physics, we may assume periodic boundary conditions and perform the Jordan-Wigner transformation $\sigma_x = e^{i\pi \sum_{x'=0}^{x-1} c_{x'}^\dagger c_{x'}} c_x$, shift the momentum of the fermions by π as $c_x \to (-1)^x c_x$, and perform a Fourier transformation $c_x = \frac{1}{\sqrt{N}} \sum_{k=0}^{N-1} q_k e^{i2\pi xk/N}$ leading to the decoupled representation of the Hamiltonian $H_{\mathrm{XX}} = \sum_k \omega_k q_k^\dagger q_k$, with $\omega_k = -4J\cos(2\pi k/N)$ the usual tight-binding or free particles on a 1D lattice dispersion relation. The correlations are then given by

$$G^{\mathrm{bulk}}_{\mathrm{XX}}(t, \beta, \mu) = \langle \sigma^\dagger(t)\sigma(0)\rangle = \lim_{N\to\infty} \frac{1}{N} \sum_k n(\omega_k) e^{i\omega_k t} = \frac{2}{N} \int_{-4J}^{4J} \frac{dk}{d\omega} n(\beta, \omega, \mu) e^{i\omega t} d\omega, \tag{C1}$$

with $\frac{dk}{d\omega} = \frac{N}{8J\pi}[1 - (\frac{\omega}{4J})^2]^{-1/2}$ and $n(\beta, \omega_k, \mu) = \mathrm{tr}\{q_k^\dagger q_k \rho_E\} = [1 + e^{\beta(\omega_k - \mu)}]^{-1}$ assuming an initial equilibrium state $\rho_E \propto e^{-\beta(H - \mu \sum_x Z_x/2)}$. At zero temperature, the mode occupation tends to the Heaviside step function $n(\beta \to \infty, \omega, \mu) = \Theta[-(\omega - \mu)]$, thus we omit β in the following. In this limit,

we can easily determine the correlations and their asymptotic ($t \gg 1$) forms collecting only the leading (slowest) power law.

For large μ, we have

$$G_{\mathrm{XX}}^{\mathrm{bulk}}(t, \mu \gg 1) = \mathcal{J}_0(4Jt) \sim \frac{\cos[\pi/4 - 4Jt]}{\sqrt{2\pi Jt}}, \tag{C2}$$

such that $\mathcal{J}_n$ is the nth order Bessel function.

Reincorporating interactions into the model, we opt to treat the large μ and arbitrary J_z regime via a first-order Holstein-Primakoff transformation [64] $Z_x = 2[1 - a_x^\dagger a_x]$ and $\sigma_x = -\sqrt{2}a_x^\dagger$. Under this approximation, the Hamiltonian takes the form

$$H_{\mathrm{XXZ}} \approx -2J \sum_x [a_x^\dagger a_{x+1} + \mathrm{H.c.}] - 4J_z \sum_x a_x^\dagger a_x, \tag{C3}$$

with a clear interpretation of J_z as a local potential or detuning with the edge sites receiving only half of the detuning of the bulk sites since they have only one neighbor. Applying the free particle techniques outlined previously, we find

$$G_{\mathrm{XXZ}}^{\mathrm{bulk}}(t, \mu \gg 1) = e^{i4J_z t} G_{\mathrm{XX}}^{\mathrm{bulk}}(t, \mu \gg 1). \tag{C4}$$

The system equilibrium correlations can also be obtained by similar techniques. We have systematically checked that our conclusions are not dependent on the initial state of the system. Therefore, for simplicity we choose to work with an initially down polarized $|\downarrow\downarrow\rangle$. The system correlation of interest is then

$$\langle \widetilde{S}_L(t) \widetilde{S}_L^\dagger(0) \rangle = \cos\left(2t\sqrt{\Delta^2 + J_S^2}\right) - \frac{i\Delta \sin\left(2t\sqrt{\Delta^2 + J_S^2}\right)}{\sqrt{\Delta^2 + J_S^2}}. \tag{C5}$$

[1] S. Hild, T. Fukuhara, P. Schauss, J. Zeiher, M. Knap, E. Demler, I. Bloch, and C. Gross, Far-From-Equilibrium Spin Transport in Heisenberg Quantum Magnets, Phys. Rev. Lett. **113**, 147205 (2014).

[2] S. Krinner, M. Lebrat, D. Husmann, C. Grenier, J.-P. Brantut, and T. Esslinger, Mapping out spin and particle conductances in a quantum point contact, Proc. Natl. Acad. Sci. USA **113**, 8144 (2016).

[3] M. Lebrat, P. Grišins, D. Husmann, Samuel Häusler, L. Corman, T. Giamarchi, J.-P. Brantut, and T. Esslinger, Band and Correlated Insulators of Cold Fermions in a Mesoscopic Lattice, Phys. Rev. X **8**, 011053 (2018).

[4] B. P. Lanyon, C. Hempel, D. Nigg, M. Muller, R. Gerritsma, F. Zahringer, P. Schindler, J. T. Barreiro, M. Rambach, G. Kirchmair *et al.*, Universal digital quantum simulation with trapped ions, Science **334**, 57 (2011).

[5] R. Blatt and C. F. Roos, Quantum simulations with trapped ions, Nat. Phys. **8**, 277 (2012).

[6] Z. Su, A. B. Tacla, M. Hocevar, D. Car, S. R. Plissard, E. P. A. M. Bakkers, A. J. Daley, D. Pekker, and S. M. Frolov, Andreev molecules in semiconductor nanowire double quantum dots, Nat. Commun. **8**, 585 (2017).

[7] D. L. Hurst, D. M. Price, C. Bentham, M. N. Makhonin, B. Royall, E. Clarke, P. Kok, L. R. Wilson, M. S. Skolnick, and A. M. Fox, Nonreciprocal transmission and reflection of a chirally coupled quantum dot, Nano Lett. **18**, 5475 (2018)

[8] T. Christen and M. Büttiker, Gauge-invariant nonlinear electric transport in mesoscopic conductors, Europhys. Lett. **35**, 523 (1996).

[9] E. Mascarenhas, D. Valente, S. Montangero, A. Auffeves, D. Gerace, and M. F. Santos, A quantum optical valve in a nonlinear-linear resonator junction, Europhys. Lett. **106**, 54003 (2014).

[10] F. Fratini, E. Mascarenhas, L. Safari, J. P. Poizat, D. Valente, A. Auffeves, D. Gerace, and M. F. Santos, Fabry-Perot Interferometer with Quantum Mirrors: Nonlinear Light Transport and Rectification, Phys. Rev. Lett. **113**, 243601 (2014).

[11] E. Mascarenhas, M. F. Santos, A. Auffeves, and D. Gerace, Quantum rectifier in a one-dimensional photonic channel, Phys. Rev. A **93**, 043821 (2016).

[12] C. Gonzalez-Ballestero, E. Moreno, F. J. Garcia-Vidal, and A. Gonzalez-Tudela, Nonreciprocal few-photon routing schemes based on chiral waveguide-emitter couplings, Phys. Rev. A **94**, 063817 (2016).

[13] K. Joulain, J. Drevillon, Y. Ezzahri, and J. Ordonez-Miranda, Quantum Thermal Transistor, Phys. Rev. Lett. **116**, 200601 (2016).

[14] Y.-J. Li, L.-Z. Lu, and X.-Y. Yu, Coherent field-controlled rectification and directional emission in a one-dimensional waveguide, J. Opt. Soc. Am. B **34**, 2317 (2017).

[15] C. Muller, J. Combes, A. R. Hamann, A. Fedorov, and T. M. Stace, Nonreciprocal atomic scattering: A saturable, quantum Yagi-Uda antenna, Phys. Rev. A **96**, 053817 (2017).

[16] Yao-Lung L. Fang and H. U. Baranger, Multiple emitters in a waveguide: Nonreciprocity and correlated photons at perfect elastic transmission, Phys. Rev. A **96**, 013842 (2017).

[17] J. Ordonez-Miranda, Y. Ezzahri, and K. Joulain, Quantum thermal diode based on two interacting spinlike systems under different excitations, Phys. Rev. E **95**, 022128 (2017).

[18] J. Dai, A. Roulet, H. N. Le, and V. Scarani, Rectification of light in the quantum regime, Phys. Rev. A **92**, 063848 (2015).

[19] A. Metelmann and A. A. Clerk, Nonreciprocal Photon Transmission and Amplification via Reservoir Engineering, Phys. Rev. X **5**, 021025 (2015).

[20] F. Fratini and R. Ghobadi, Full quantum treatment of a light diode, Phys. Rev. A **93**, 023818 (2016).

[21] D. Roy, Critical features of nonlinear optical isolators for improved nonreciprocity, Phys. Rev. A **96**, 033838 (2017).

[22] H. Z. Shen, Y. H. Zhou, and X. X. Yi, Quantum optical diode with semiconductor microcavities, Phys. Rev. A **90**, 023849 (2014).

[23] A. Purkayastha, A. Dhar, and M. Kulkarni, Non-linear transport in an out-of-equilibrium single-site Bose Hubbard model: Scaling, rectification and time dynamics, Phys. Rev. A **94**, 052134 (2016).

[24] A. Rosario Hamann, C. Muller, M. Jerger, M. Zanner, J. Combes, M. Pletyukhov, M. Weides, T. M. Stace, and A. Fedorov, Nonreciprocity Realized with Quantum Nonlinearity, Phys. Rev. Lett. **121**, 123601 (2018).

[25] S. Lepri and G. Casati, Asymmetric Wave Propagation in Nonlinear Systems, Phys. Rev. Lett. **106**, 164101 (2011).

[26] K. A. van Hoogdalem and D. Loss, Rectification of spin currents in spin chains, Phys. Rev. B **84**, 024402 (2011).

[27] B. Braunecker, D. E. Feldman, and J. B. Marston, Rectification in one-dimensional electronic systems, Phys. Rev. B **72**, 125311 (2005).

[28] L. Zhang, Y. Yan, C. Q. Wu, J. S. Wang, and B. Li, Reversal of thermal rectification in quantum systems, Phys. Rev. B **80**, 172301 (2009).

[29] J. Thingna and J. S. Wang, Spin rectification in thermally driven XXZ spin chain via the spin-Seebeck effect, Europhys. Lett. **104**, 37006 (2013).

[30] D. Segal, Single Mode Heat Rectifier: Controlling Energy Flow between Electronic Conductors, Phys. Rev. Lett. **100**, 105901 (2008).

[31] Z. Wei, M. Kondratenko, L. H. Dao, and D. F. Perepichka, Rectifying diodes from asymmetrically functionalized single-wall carbon nanotubes, J. Am. Chem. Soc. **128**, 3134 (2006).

[32] Z. Lenarcic and T. Prosen, Exact asymptotics of the current in boundary-driven dissipative quantum chains in large external fields, Phys. Rev. E **91**, 030103(R) (2015).

[33] G. T. Landi, E. Novais, M. J. de Oliveira, and D. Karevski, Flux rectification in the quantum XXZ chain, Phys. Rev. E **90**, 042142 (2014).

[34] L. Schuab, E. Pereira, and G. T. Landi, Energy rectification in quantum graded spin chains: Analysis of the XXZ model, Phys. Rev. E **94**, 042122 (2016).

[35] E. Pereira, Rectification and one-way street for the energy current in boundary-driven asymmetric quantum spin chains, Phys. Rev. E **95**, 030104(R) (2017).

[36] E. Pereira, Requisite ingredients for thermal rectification, Phys. Rev. E **96**, 012114 (2017).

[37] V. Balachandran, G. Benenti, E. Pereira, G. Casati, and D. Poletti, Perfect Diode in Quantum Spin Chains, Phys. Rev. Lett. **120**, 200603 (2018).

[38] E. Pereira, Heat, work, and energy currents in the boundary-driven XXZ spin chain, Phys. Rev. E **97**, 022115 (2018).

[39] T. Werlang, M. A. Marchiori, M. F. Cornelio, and D. Valente, Optimal rectification in the ultrastrong coupling regime, Phys. Rev. E **89**, 062109 (2014).

[40] D. Malz and A. Nunnenkamp, Current rectification in a double quantum dot through fermionic reservoir engineering, Phys. Rev. B **97**, 165308 (2018).

[41] A. Braggio, J. Konig, and R. Fazio, Full Counting Statistics in Strongly Interacting Systems: Non-Markovian Effects, Phys. Rev. Lett. **96**, 026805 (2006).

[42] C. Flindt, T. Novotny, A. Braggio, M. Sassetti, and A.-P. Jauho, Counting Statistics of Non-Markovian Quantum Stochastic Processes, Phys. Rev. Lett. **100**, 150601 (2008).

[43] K. H. Thomas and C. Flindt, Electron waiting times in non-Markovian quantum transport, Phys. Rev. B **87**, 121405(R) (2013).

[44] J. Cerrillo, M. Buser, and T. Brandes, Nonequilibrium quantum transport coefficients and transient dynamics of full counting statistics in the strong-coupling and non-Markovian regimes, Phys. Rev. B **94**, 214308 (2016).

[45] X. Zheng, J. Luo, J. Jin, and Y. Yan, Complex non-Markovian effect on time-dependent quantum transport, J. Chem. Phys. **130**, 124508 (2009).

[46] J. Jin, X.-Q. Li, M. Luo, and Y. Yan, Non-Markovian shot noise spectrum of quantum transport through quantum dots, J. Appl. Phys. **109**, 053704 (2011).

[47] A. Lofgren, C. A. Marlow, I. Shorubalko, R. P. Taylor, P. Omling, L. Samuelson, and H. Linke, Symmetry of Two-Terminal Nonlinear Electric Conduction, Phys. Rev. Lett. **92**, 046803 (2004).

[48] J. Schulenborg, J. Splettstoesser, and M. R. Wegewijs, Duality for open fermion systems: Energy-dependent weak coupling and quantum master equations, Phys. Rev. B **98**, 235405 (2018).

[49] R. G. Pereira, S. R. White, and I. Affleck, Spectral function of spinless fermions on a one-dimensional lattice, Phys. Rev. B **79**, 165113 (2009).

[50] I. S. Eliens, F. B. Ramos, J. C. Xavier, and R. G. Pereira, Boundary versus bulk behavior of time-dependent correlation functions in one-dimensional quantum systems, Phys. Rev. B **93**, 195129 (2016).

[51] T. Giamarchi, *Quantum Physics in One Dimension* (Oxford University Press, Oxford, UK, 2004).

[52] A. Kadlecová, Ma. Žonda, and T. Novotný, Quantum dot attached to superconducting leads: Relation between symmetric and asymmetric coupling, Phys. Rev. B **95**, 195114 (2017).

[53] G. D. Mahan, *Many-Particle Physics* (Plenum Press, New York, 1990).

[54] R. Kubo, Statistical-mechanical theory of irreversible processes. I: General theory and simple applications to magnetic and conduction problems, J. Phys. Soc. Jpn. **12**, 570 (1957).

[55] R. Kubo, The fluctuation-dissipation theorem, Rep. Prog. Phys. **29**, 255 (1966).

[56] R. Kubo, M. Toda, and N. Hashitsume, *Statistical Physics II* (Springer, Berlin, 1985).

[57] M. T. Mitchison and M. B. Plenio, Non-additive dissipation in open quantum networks out of equilibrium, New J. Phys. **20**, 033005 (2018).

[58] H. J. Carmichael, *Statistical Methods in Quantum Optics 1* (Springer, Berlin, 1999).

[59] H.-P. Breuer and F. Petruccione, *The Theory of Open Quantum Systems* (Oxford University Press, Oxford, 2002).

[60] A. Purkayastha, A. Dhar, and M. Kulkarni, Out-of-equilibrium open quantum systems: A comparison of approximate quantum master equation approaches with exact results, Phys. Rev. A **93**, 062114 (2016).

[61] P. P. Hofer, M. Perarnau-Llobet, L. David, M. Miranda Haack, R. Silva, J. B. Brask, and N. Brunner, Markovian master equations for quantum thermal machines: Local versus global approach, New J. Phys. **19**, 123037 (2017).

[62] J. Onam Gonzalez, L. A. Correa, G. Nocerino, J. P. Palao, D. Alonso, and G. Adesso, Testing the validity of the local and global GKLS master equations on an exactly solvable model, Open Syst. Inform. Dyn. **24**, 1740010 (2017).

[63] D. Jaschke, L. D. Carr, and I. de Vega, Thermalization in the quantum Ising model–Approximations, limits, and beyond, arXiv:1805.04934.

[64] T. Holstein and H. Primakoff, Field dependence of the intrinsic domain magnetization of a ferromagnet, Phys. Rev. **58**, 1098 (1940).

[65] A. Gonzalez-Tudela and J. I. Cirac, Quantum Emitters in Two-Dimensional Structured Reservoirs in the Nonperturbative Regime, Phys. Rev. Lett. **119**, 143602 (2017).

[66] K. Bidzhiev and G. Misguich, Out-of-equilibrium dynamics in a quantum impurity model: Numerics for particle transport and entanglement entropy, Phy. Rev. B **96**, 195117 (2017).

[67] J. J. Garcia-Ripoll, Time evolution algorithms for matrix product states and DMRG, New J. Phys. **8**, 305 (2006).

[68] T. Koffel, M. Lewenstein, and L. Tagliacozzo, Entanglement Entropy for the Long-Range Ising Chain in a Transverse Field, Phys. Rev. Lett. **109**, 267203 (2012).

[69] P. Hauke and L. Tagliacozzo, Spread of Correlations in Long-Range Interacting Quantum Systems, Phys. Rev. Lett. **111**, 207202 (2013).

[70] J. Schachenmayer, B. P. Lanyon, C. F. Roos, and A. J. Daley, Entanglement Growth in Quench Dynamics with Variable Range Interactions, Phys. Rev. X **3**, 031015 (2013).

[71] A. S. Buyskikh, M. Fagotti, J. Schachenmayer, F. Essler, and A. J. Daley, Entanglement growth and correlation spreading with variable-range interactions in spin and fermionic tunneling models, Phys. Rev. A **93**, 053620 (2016).

[72] J. Haegeman, J. I. Cirac, T. J. Osborne, I. Pizorn, H. Verschelde, and F. Verstraete, Time-Dependent Variational Principle for Quantum Lattices, Phys. Rev. Lett. **107**, 070601 (2011).

[73] J. Haegeman, C. Lubich, I. Oseledets, B. Vandereycken, and F. Verstraete, Unifying time evolution and optimization with matrix product states, Phys. Rev. B **94**, 165116 (2016).

[74] V. Zauner-Stauber, L. Vanderstraeten, M. T. Fishman, F. Verstraete, and J. Haegeman, Variational optimization algorithms for uniform matrix product states, Phys. Rev. B **97**, 045145 (2018).

[75] H. N. Phien, G. Vidal, and I. P. McCulloch, Infinite boundary conditions for matrix product state calculations, Phys. Rev. B **86**, 245107 (2012).

[76] F. Schwarz, M. Goldstein, A. Dorda, E. Arrigoni, A. Weichselbaum, and J. von Delft, Lindblad-driven discretized leads for non-equilibrium steady-state transport in quantum impurity models: Recovering the continuum limit, Phys. Rev. B **94**, 155142 (2016).

[77] E. Mascarenhas, Research data for "Nonreciprocal Quantum Transport at Junctions of Structured Leads," University of Strathclyde, doi:10.15129/1a689315-46ec-4487-be26-672f2e221fea (2019).

[78] H. M. Wiseman and G. J. Milburn, *Quantum Measurement and Control* (Cambridge University Press, Cambridge, UK, 2010).